DTU Library

Experimental and Numerical study of Wake to Wake Interaction in Wind Farms

Machefaux, Ewan; Troldborg, Niels; Larsen, Gunner Chr.; Mann, Jakob; Aagaard Madsen , Helge

Experimental and Numerical study of Wake to Wake Interaction in Wind Farms

Ewan Machefaux, Niels Troldborg, Gunner C. Larsen,
Jakob Mann and Helge Aa. Madsen

Technical University of Denmark, Risø Campus, Department of Wind Energy
Building VEA-118, P.O box 49, DK-4000 Roskilde, Denmark
email: ewma@dtu.dk

Abstract:

In this paper, wake interaction between two wind turbines is analyzed using experimental and numerical approaches. Full-scale wake measurements are conducted at Tjæreborg wind farm and are obtained using a continuous wave lidar mounted on the back of the nacelle of a 2MW NM80 turbine. Numerical analyses are conducted for two double wake cases characterized by different turbine spacing, using the in-house EllipSys3D flow solver. Large Eddy Simulation and Actuator Line technique are used for modeling the rotor and the flow field. 10-minute average streamwise velocity and turbulence level are compared, and good agreement is seen between the measurements and the computations despite of a lateral offset and other discrepancies due to uncertainties on the measured inflow conditions and lidar mounting alignment.

Keywords: remote sensing; lidar; wind turbine wake; CFD; Large Eddy Simulation; Actuator Line Method;

1 Introduction

Modeling the complex flow fields observed in a wind farm has become one of the most prioritized topics of wind energy research in the past decade. The complexity of wind farm flow fields is not only due to the highly turbulent nature of the wake, but also influenced by its interaction with other wakes and the atmospheric boundary layer.

Today, the model of Frandsen [1] is used in the design standards for wind turbines in wind farms. In this model the power production of turbines in a wind farm is predicted based on 1D momentum considerations similar to the work of Jensen [2], while the fatigue loading is based on the so-called effective turbulence intensity, [1]. The model of Frandsen works in general well but occasionally reveals discrepancies when compared to measurements.

Recently Ott et al. developed the FUGA model [3], which is a very fast linearized CFD model tool for simulation of wind farm wakes. This model was used to predict the power output from the Horns Reef and Nysted wind farms and revealed good agreement when compared with measurements. However, because FUGA is a steady state model, it is not well suited for predicting loads.

In order to formulate a fast unifying theory that account for both power production and loads on wind turbines in wind farms, Larsen et al. developed a "poor man's" LES, i.e. the unsteady Dynamic Wake Meandering model [4], where the main assumption is, that the wake meandering is governed by large scale turbulence structures in the atmosphere. This interpretation is supported by lidar measurements by Bingöl et al. [5] as well as by hot wire and PIV measurements in a boundary layer wind tunnel conducted by España et al. [6]. The DWM model has previously proven accurate for predicting single wake development [7], but recently also for predicting power output and loads of a whole wind farm when combined with the aero-elastic code HAWC2 and suitable assumptions about merging wakes, [8]. Despite the promising results of the DWM model there is still room for improvements in terms of wake deficit and turbulence characteristics, which are derived assuming axisymmetry of the wake. For future improvement, a better understanding of the characteristics of merged wakes is necessary.

With the newest remote sensing technology such as lidars, both industry and research community can now benefit from detailed full-scale measurements of wakes, giving a large and valuable source of knowledge for deeper analysis and model validation of wake generation, development and interaction. Specifically, two-dimensional lidar scanning of wakes have been conducted by Larsen et al. [9] on a stall regulated 95kW Tellus turbine at Risø and on a 2MW wind turbine at the Tjæreborg site to characterize the wake meandering as well as the quasi-steady wake deficit and wake turbulence under real atmospheric conditions.

Wake interaction and characteristics have also been studied extensively using computational fluid dynamic. Fletcher and Brown [10] simulated the aerodynamic interaction between two wind turbines

operating in uniform flow conditions using a lifting line technique. Troldborg et al. [11], Storey et al. [12] and Lee et al. [13] used the actuator line model to simulate wake interaction between two turbines operating in the atmospheric boundary layer. In the latter study the influence of both roughness and atmospheric stability was investigated and shown to be of major importance for turbine loads and power production. Simulations of a whole wind farm have been carried out by Ivanell [14] using the actuator disc method as well as by Churchfield et al. [15] using the actuator line model. Such simulations provide valuable information about wakes and can be used to calibrate simpler engineering models [7].

The present paper is a continuation of the study of Troldborg et al. [11]. It aims to contribute to the overall understanding of two interacting wakes, also referred to as double wake, by the use of lidar measurement recorded from the nacelle of a modern 2MW turbine combined with a numerical study of the same turbine exposed to similar external flow field conditions. This numerical study, similar to the one conducted in [11], uses the Risø DTU in-house 3D Navier-Stokes solver EllipSys3D. Analysis and comparison of merged wake characteristics is performed for two different turbine spacings and inflow conditions. It is a one to one mapping of experimental results on numerical predictions.

2   Experimental approach

The experimental data were obtained from a full-scale experiment conducted at Tjæreborg Enge wind farm, as part of the EU-TOPFARM project [16]. It is an onshore wind farm located south of the city of Esbjerg and approximately 15km from the west coast of Denmark. The site is open land with low roughness; it has thus typically low shear and low turbulence for the prevailing westerly winds. The layout of the wind farm is sketched in Figure 1. During the measurement campaign, the NEG MICON NM80 wind turbine denoted WT3 was instrumented with a nacelle mounted lidar, which scanned 2D flow fields in its wake at different downstream cross sections. A ZephIR Continuous Wave lidar system manufactured by QinetiQ was adapted to comply with the specific project needs and details of this equipment and its adaptation can be found in [5]. The level of uncertainties associated with lidar anemometry has been studied by Lindelöw-Marsden [17], and it is likely that a ZephIR equipment can extract the wind velocity with a deviation of $\pm 2\%$ when compared with cup anemometers. The lidar measurements were synchronized with simultaneous 20 Hz wind field measurements from the nearby 93 m high intensively instrumented reference mast (M1), as well as with 1 Hz

measurement on WT3 of various operational conditions (yaw, power, rotor speed and pitch).
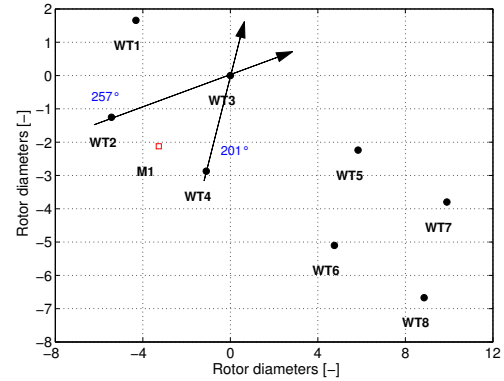

Figure 1: Tjæreborg wind farms and selected main wake directions. The graphic is scaled based on rotor diameters (80m). The wind farm consists of 3 Vestas V80-2MW and 5 NEG MICON NM80 turbines owned by DONG Energy A/S and Vatenfall AB, respectively

As a part of the experimental analysis, the rotor wake longitudinal flow field is discretized by associating lidar cross sectional recordings with non-overlapping grid cells of $2 \times 10m^2$ from a particular laser beam sweep. By averaging all measurements within a cell for each "passage", the flow field statistics will appear on a regular grid. The lidar is averaging the velocities along the beam over a distance which depend on the range. This distance (≈ 50m at focus distance of 200m) is significantly larger than the grid cells, thus in turn justifying the applied cell averaging. An illustration of a typical lidar sweep pattern and the corresponding averaging grid is shown on Fig. 2(a). Fig. 2(b) shows the measurements spherical envelop defined by the lidar focus distance, viewed from the top.

The subsequent analysis involves 2 merged wake situations: 1) the double wake from wind turbines WT2/WT3 with a large turbine spacing ($\approx 5.5D$); and 2) the double wake from wind turbines WT4/WT3 with a lower turbine spacing ($\approx 3D$). The comparison is conducted using 10-minute averaged time series associated with a 200m downstream focus distance. In order to mimic the experimental conditions, the computed data are obtained using specific measured ambient conditions as listed in Table 1 (cf. Section 3). Both 10-minutes measurements have a neutral atmospheric stability class (obtained with the use of temperature sensors and computed with the Monin-Obukhov similarity theory). Finally, the 10-minutes average wind direction is equal to the ideal full wake direction, and its standard deviation does not exceed $5°$ in both cases.
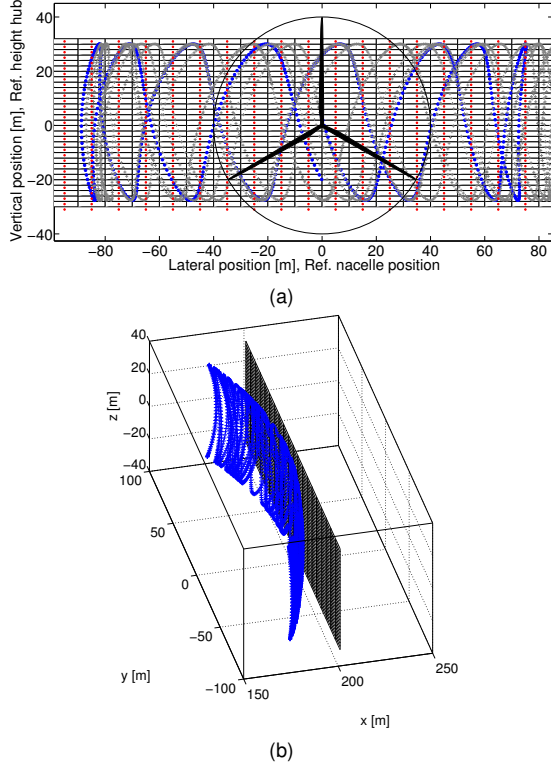
Figure 2: (a) lidar wake resolving grid at a focus distance of 200m ($\approx 2.5D$). The blue dots represent one sweep pattern, the gray crosses are consecutive sweeps. The superposed resolving grid is also shown with its cell centers in red circle. (b) View from the top and expressed in the lidar axis coordinate (x-axis is the flow direction)

In order to perform a fair comparison between the main flow direction component U from the computations and the line of sight velocity (U_{los}) from the laser beam, an additional correction is proposed. The angle between the laser beam and the main flow direction (z-axis) can increase significantly outside of the wake core. We denote the instantaneous flow velocity vector expressed in the fixed frame of reference by:

$$(v(t), w(t), U + u(t)) \equiv \underline{U}(t) \qquad (1)$$

where U is the mean streamwise velocity in the wake, u(t) is the fluctuating longitudinal part, v(t) is the fluctuating lateral part, and w(t) is the fluctuating vertical part. Similarly, we denote the instantaneous flow velocity vector expressed in the lidar beam frame of reference by:

$$\left(\tilde{v}(t), \tilde{w}(t), \tilde{U}(t) + \tilde{u}(t) \right) \equiv \underline{\tilde{U}}(t) \qquad (2)$$

As previously shown on Fig. 2(a), the lidar beam is moving with 2 degrees of freedom in the fixed frame of reference. The pan angle, denoted θ_P, represents the beam angle resulting from the rotation around the

Table 1: Case study 10min average quantities

Site measurements	WT2-WT3	WT4-WT3
Wind speed [m/s]	8.50	7.24
Shear coef. [-]	0.14	0.08
Inflow turbulence level [-]	0.05	0.03
RPM upstream [-]	15.00	15.90
RPM downstream [-]	13.15	12.22
Turbine separation [m]	446	246
lidar Focus distance [m]	200	200

x-axis (illustrated in Fig. 3), whereas the tilt angle θ_T is the rotation angle around the y-axis.
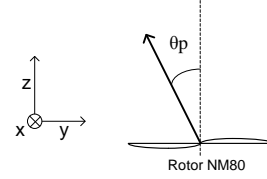

Figure 3: Representation of the pan angle of the laser beam in the fixed frame of reference

The transformation matrix defining a panning, $\theta_P(t)$, of the fixed frame of reference is:

$$\underline{\underline{T}}_P \equiv \begin{pmatrix} 1 & 0 & 0 \\ 0 & \cos\theta_P(t) & -\sin\theta_P(t) \\ 0 & \sin\theta_P(t) & \cos\theta_P(t) \end{pmatrix} \qquad (3)$$

Similarly, the transformation matrix associated with tilting the fixed frame of reference is:

$$\underline{\underline{T}}_T \equiv \begin{pmatrix} \cos\theta_T(t) & 0 & \sin\theta_T(t) \\ 0 & 1 & 0 \\ -\sin\theta_T(t) & 0 & \cos\theta_T(t) \end{pmatrix} \qquad (4)$$

with $\theta_T(t)$ denoting the tilt angle. The velocity vector $\underline{U}$ can be transformed to the lidar beam frame of reference by calculating the product $\underline{\tilde{U}} = \underline{\underline{T}}_P \underline{\underline{T}}_T \underline{U}$:

$$\underline{\tilde{U}} = \begin{pmatrix} w(t)\cos\theta_T(t) + (U + u(t))\sin\theta_T(t) \\ v(t)\cos\theta_P(t) + w(t)\sin\theta_P(t)\sin\theta_T(t) \\ \cdots - (U + u(t))\sin\theta_P(t)\cos\theta_T(t) \\ v(t)\sin\theta_P(t) - w(t)\cos\theta_P(t)\sin\theta_T(t) \\ \cdots + (U + u(t))\cos\theta_P(t)\cos\theta_T(t) \end{pmatrix} \qquad (5)$$

The line-of-sight velocity U_{los} is expressed as:

$$U_{los} \equiv \tilde{U}(t) + \tilde{u}(t) \qquad (6)$$
$$= v(t)\sin\theta_P(t) - w(t)\cos\theta_P(t)\sin\theta_T(t)$$
$$+ (U + u(t))\cos\theta_P(t)\cos\theta_T(t)$$

For moderate tilt and pan angles and for a conventional atmospheric boundary layer, the following conditions apply:

1. $v(t) \sin \theta_P(t) \ll (U + u(t)) \cos \theta_P(t) \cos \theta_T(t)$

2. $w(t) \sin \theta_T(t) \ll (U + u(t)) \cos \theta_T(t)$

Thereby, the z- component of Eq. (5) reduces to:

$$
\begin{aligned}
U_{los}(t) &\simeq (U + u(t)) \cos \theta_P(t) \cos \theta_T(t) \\
(U + u(t)) &\simeq U_{los}(t) \cdot \frac{1}{\cos \theta_P(t) \cos \theta_T(t)}
\end{aligned}
$$
(7)

To conclude, the projection of U_{los} along the streamwise velocity in the fixed frame of reference is computed as:

$$
U_{lidar}(t) = U_{los}(t) \cdot \frac{1}{\cos \arcsin \left(\frac{Y}{FC} \right) \cos \arcsin \left(\frac{X}{FC} \right)}
$$
(8)

where X and Y are vertical and horizontal position of the beam, respectively, and FC is the lidar focus distance. A 2D representation of the correction for the pan angle is shown on Fig. 4.
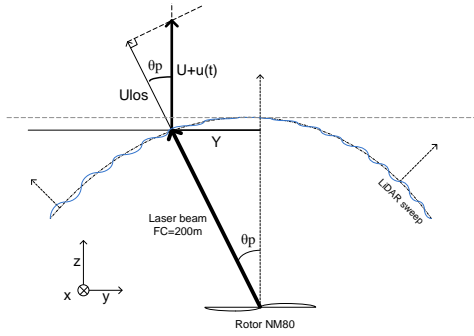

Figure 4: Velocity triangle for a lidar measurement. The line of sight velocity (U_{los}) is projected on the main flow direction for comparison with numerical computations.

Finally, as opposed to the analysis conducted in [18], the present analysis of the wake is done in a fixed frame of reference to simplify matters, due to the complexity of implementing a meandering tracking algorithm for merged wakes. This will be the subject for later research as part of the FlowCenter project, involving a new full-scale experiment conducted at DTU Risø campus.

3   Numerical approach

The computation of the flow field has been carried out by Large Eddy Simulation (LES) approach using the 3D flow solver EllipSys3D developed by Michelsen and Sørensen [19], [20]. The wind turbine rotor is simulated using the actuator line model developed by Sørensen and Shen [21]. The modelling of the atmospheric boundary layer (ABL) is done in two parts: a model for the sheared atmospheric mean velocity field and a model for the ambient turbulence. The mean velocity field is imposed using a technique where steady body forces are initially computed and applied to the entire domain, while synthetic turbulent fluctuations are introduced in a cross-section upstream of the rotors by using an unsteady actuator.

The turbulence field is generated prior to the computation using the Mann algorithm [22], which produces homogeneous, stationary, Gaussian and anisotropic turbulence with the same spectral characteristics as observed in the neutral atmosphere. The unsteady computation are performed until at least 10 minutes average statistic of the wake flow can be extracted and compared to the measurements.

Two Cartesian computational domains have been used in the present study: one for the case with $3D$ spacing; and one for the $5.5D$ spacing. The grid layout and boundary conditions are in accordance with previous studies on wake computation [11], where the inlet is applied with the desired wind shear profile; the outlet has unsteady convective conditions; the ground of the domain has a wall no slip condition; and the top boundary is set to the farfield velocity. The dimensions of the grid used for the $5.5D$ spaced turbines is (L_x, L_y, L_z): ($24R$, $24R$, $37.4R$) while the one for the $3D$ spacing is ($24R$, $24R$, $31.8R$), where L_z denotes the length in flow direction, L_y the domain height, and L_x the domain width, and R is the rotor radius. The two grids have 3.981 and 2.949 millions cells, respectively. The cells are in both grids concentrated equidistantly with a spacing of 0.04R in the region around and between the turbines in order to resolve and preserve the wake structures. An overview of the computational domain is shown in Fig. 5(a) for the y-z plane and in Fig. 5(b) for the x-y plane. Note that only every 16th cell boundary is shown in the Figures.

4   Results and discussion

4.1   Merged wake at 2.5D downstream for 3D turbine spacing

The average wake characteristics at hub height 2.5D downstream of WT3 when operating fully in the wake of WT4 (i.e. 3D spacing) is shown in Fig. 6. A first computation conducted with the same parameters as measured on the mast M1 showed poor agreement with the measured deficit as seen on Fig. 6(a). The streamwise wake velocity extracted from the computation is everywhere larger than the measured one, which might be a consequence of a possible over estimation of the inflow wind speed. Moreover, the computed power of both turbines is not consistent
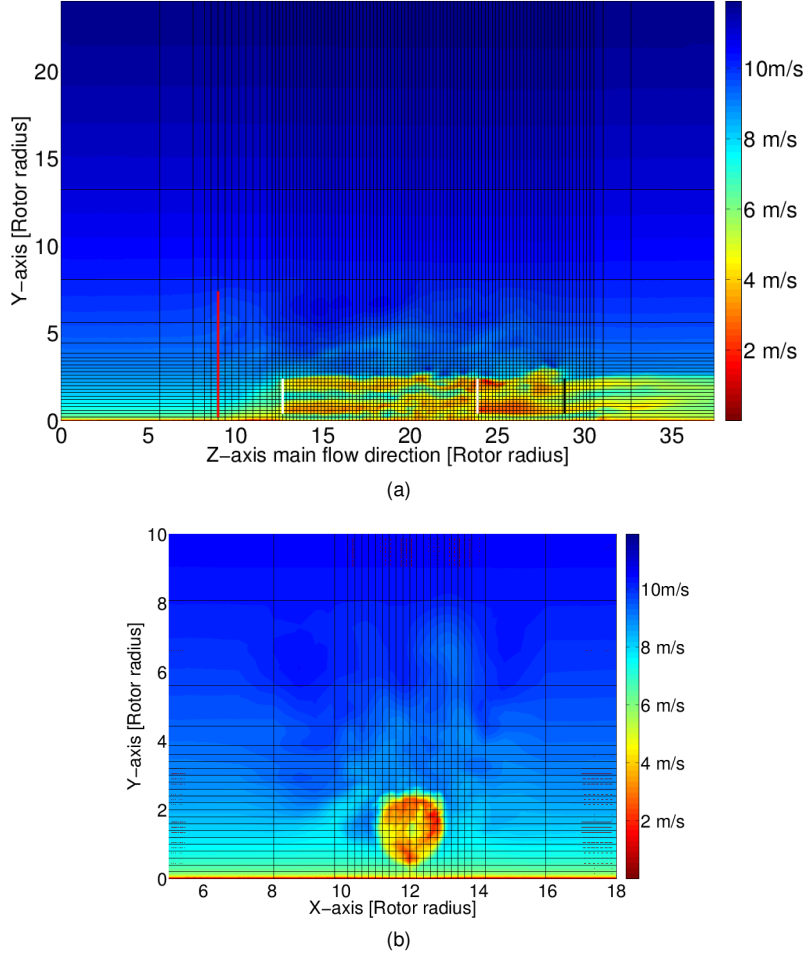
Figure 5: Overview of the computational domain. (a) Average streamwise velocity field extracted from a cross section in the middle of the domain ($L_x = 12R$). The red plane ($L_z = 9.2R$) indicates the location of introduced turbulence generated using the Mann model prior to the computations. The location of the two turbines are symbolized by the white planes. Finally the location of the lidar recording plane is shown in black. (b) Average streamwise velocity field extracted from a reduced size cross section ($L_z = 24R$).

with neither the NM80 power curve nor their respective measured power. This confirms that the wind speed measured at the mast is not representative for the actual upstream rotor wind speed, which explains the discrepancies previously observed on Fig. 6. Additionally, the RPM of the upwind turbine is not known accurately, due to the fact that only integer variables were used for this sensor recording in the database.

Consequently, a sensitivity analysis is performed where RPM, turbulence level and inflow velocity are slightly changed around the measured values. For each case, the relative error on the power production (as defined by Eq. (9)) is investigated, and the results are summarized in Table 2.

$$\epsilon = 100 \cdot \frac{P_{EllipSys3D} - P_{meas}}{P_{EllipSys3D}} \qquad (9)$$

With reference to Fig. 6, it is seen that the best wake velocity and turbulence level agreement ob-

Table 2: Relative error on power production

TI [%]; U0 [m/s]; RPM [-]	Rel. error WT4 [%]	Rel. error WT3 [%]	Rel. error power ratio [%]
5%; 8.5m/s; 15 (measured)	13.20	18.34	5.92
10%; 8.5m/s; 15	5.52	35.16	31.37
5%; 7.0m/s; 15	-56.03	-47.60	5.41
5%; 7.0m/s; 17	-47.04	-34.74	8.37
5%; 8.5m/s; 17	9.14	19.10	10.97
5%; 8.0m/s; 15	-2.84	3.43	6.09

tained for computations with a free stream velocity of 7.0 m/s. However, for the two RPM-cases associated with this wind speed, large deviations of around 50% are observed on the power production, as seen in Table 2. This emphasizes the sensitivity of the power production with respect to a change in wind speed, since the power is function of the cube of the free-stream velocity.

The minimum wake wind speed has the best agreement with the computation performed at 8.0 m/s under the same RPM and turbulence level setting as measured. Also both mechanical power and power ratio have a deviation of less than 4% from the measurement. For this case, the agreement remains less convincing outside the core of the wake, where the wind speed recovery is less abrupt in the measurement. The measured wake center location deviates from the computed one with a lateral offset of magnitude 10-12m. The analysis suffers from the lack of knowledge of the measured wind speed outside of the wake, due to the limitations in the lidar spatial coverage. This deviation may be a consequence of the influence of a nearby turbine, uncertainties of the yaw misalignment of the turbines, or other mounting issues. Moreover, it must be stated that discrepancies exists while comparing only one 10-minute timeserie with another, due to natural variability. Finally, it is also possible that the meandering of the wake in the LES computations is too low due to the "limited" size of the turbulence box in the lateral direction. In the work conducted by Madsen et al. [7], the turbulence box is extended to several kilometers.

Additionally, contour plots of the measured and computed streamwise wake velocities (corresponding to $U_0 = 8.0 m/s$) are shown on Fig. 7, and similarly the turbulence level are shown on Fig. 8. It is seen on Fig. 7(a), that the measured wake has a more rapid transition into a bell shaped form and is more asymmetric than the computed wake for the given downstream position. Finally, the measured wake has a larger expansion, maybe due to meander, which is clearly seen in Fig. 6(b).

4.2 Merged wake at 2.5D downstream for 5.5D turbine spacing

Similar analysis is conducted for the wake interaction of turbines WT3 and WT2 as shown on Fig. 9. In this case, the recorded overall wake wind speed and turbulence level shapes are in very good agreement with the computations as is the power produced. Once again, a lateral offset is clearly seen in the mean profile. At 200m downstream, this offset is of the order of 10 to 15m in both cases, corresponding to an angle of $2.9\,°$ to $4.2\,°$ at the nacelle. Because of the moderate magnitude of this angle, the observed offset could realistically be the consequence of a small mounting misalignment of the lidar beam axis to the nacelle axis.

The comparison of contour plots of wake velocity and turbulence profile shows similar discrepancies as observed for the lower turbine spacing case;
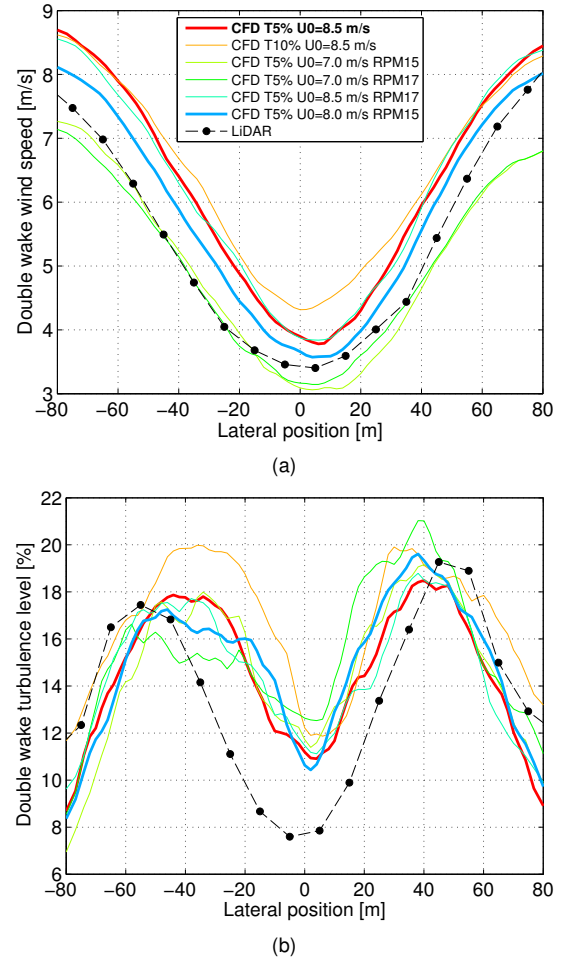

Figure 6: Comparison of (a) measured (lidar) and computed (CFD) stream wise wake velocity; and (b) turbulence intensity at hub height for the double wake situation generated by WT4 and WT3. The bold text in the legend corresponds to the computation using the measured ambient condition which shows poor agreement with the full-scale flow recordings. The dots represent full-scale measurements.

i.e. the measured wake has a larger expansion and more pronounced asymmetry as compared to the computed one. In both cases, the turbulence profile seen on Fig. 6(b) and Fig. 9(b), respectively, has a non symmetric profile, which most likely relates to the combined wake rotation and shear, as described in the study by Zahle and Sørensen [23]. The turbulence level around the wake core is less than the computed one, and this could be the consequence of the spatial averaging of the lidar.

A quantitative measure of the previous comparisons is given by the cross correlation coefficient R with respect to the lateral position X denoted $R(X)$. When considering deficit and turbulence profiles as data series, the normalized cross correlation coefficient, ρ, of the two random variables $(D_m; D_p)$ repre-

senting the measured and predicted wake velocity, is given by:

$$\rho(X) = \frac{R(X)}{\sigma_{D_m}\sigma_{D_p}} \qquad (10)$$

$$= \frac{E\left[(D_m(x+X)-<D_m>)(D_p(x)-<D_p>)\right]}{\sigma_{D_m}\sigma_{D_p}}$$

The formulation is similar in the case of the turbulence level represented by an analog couple of "random variables" $(T_m; T_p)$. E is the expected value operator, X is the lateral position in meter, σ_D is the standard deviation of the deficit, $<D>$ refers to the average of the deficit in space, and subscripts m and p refer to measured and predicted, respectively. For each case, the maximum normalized cross correlation coefficient is found at a particular lateral offset. The results of this analysis are summarized in Table 3. From Table 3, it is seen that the magnitude of the lateral offset is nearly constant for the two cases, reinforcing the conjecture of having a combination of yaw and lidar mounting misalignment. The cross correlation coefficient is very close to 1, indicating a high correlation between the data series analyzed and therefore good agreements in the comparison.

Table 3: Normalized cross correlation coefficients and corresponding lateral offsets.

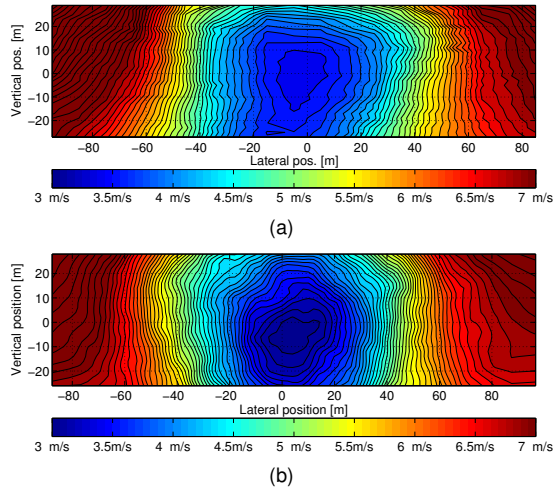|	Turb. WT4-WT3	Turb. WT4-WT3	Ws WT2-WT3	Ws WT2-WT3
$\rho(X)$ [-]	0.979	0.982	0.984	0.988
X [m]	5	6	6	7

Figure 7: Comparison of (a) measured (lidar); and (b) computed (CFD) contour plot of streamwise wake velocity for the double wake situation generated by WT4 and WT3.
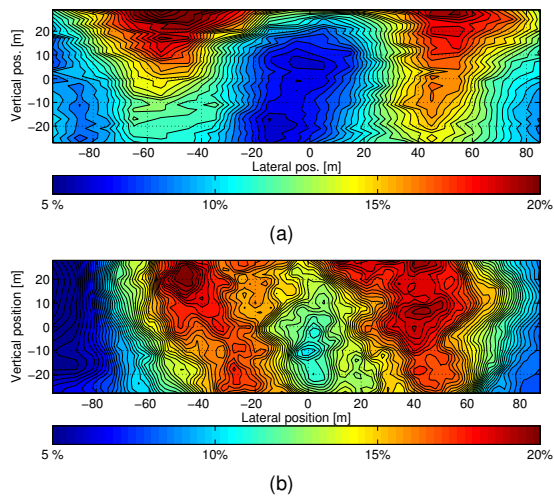

Figure 8: Comparison of (a) measured (lidar); and (b) computed (CFD) contour plot of wake turbulence level for the double wake situation generated by WT4 and WT3.
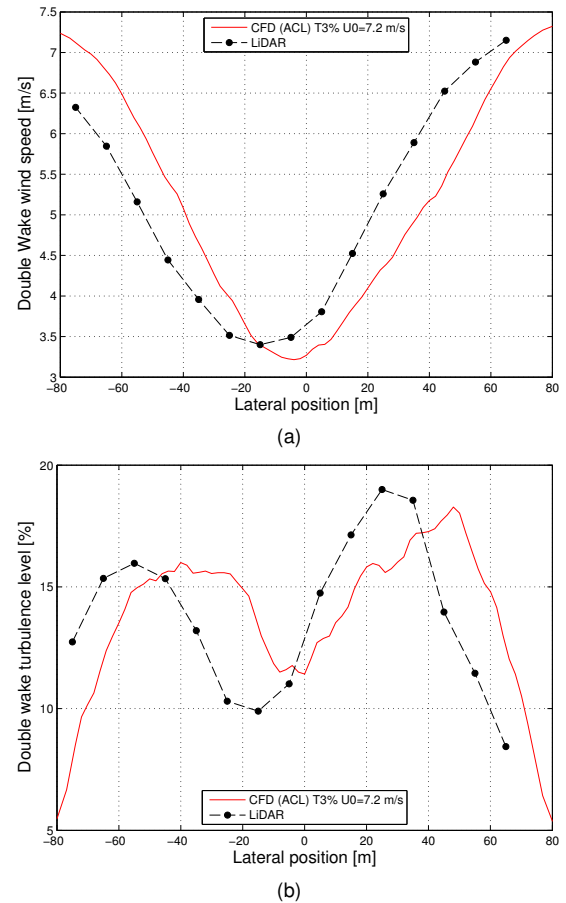

Figure 9: Comparison of (a) measured (lidar) and computed (CFD) stream wise wake velocity; and (b) turbulence intensity at hub height for the double wake situation generated by WT2 and WT3. The dots represent full-scale measurements.
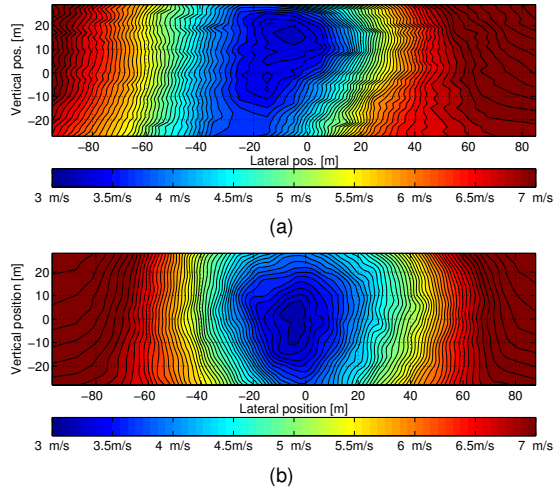
Figure 10: Comparison of (a) measured (lidar); and (b) computed (CFD) contour plot of streamwise wake velocity for the double wake situation generated by WT2 and WT3.
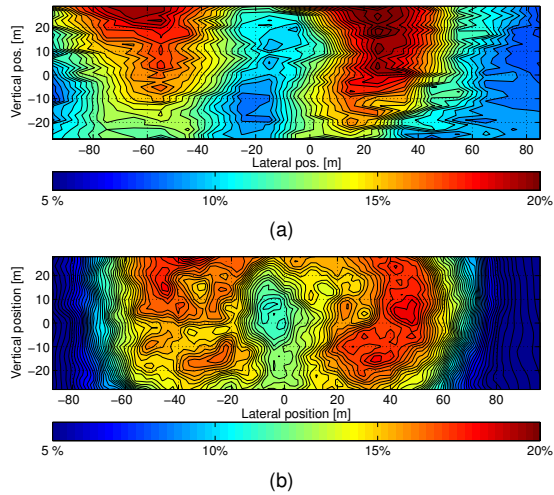

Figure 11: Comparison of (a) measured (lidar); and (b) computed (CFD) contour plot of wake turbulence level for the double wake situation generated by WT2 and WT3.

5 Conclusion

In the present analysis, two wind turbine double wake cases are investigated using full-scale experimental data and CFD LES ACL computations on a NM80 turbine in the Tjæreborg wind farm. A sensitivity analysis is performed to enhance agreement and to overcome the uncertainties related to the recording of ambient wind field conditions and turbine sensors. A lateral offset between the wake variance profiles is observed, which may be a consequence of either a calibration issue on the yaw sensor or a misalignment of the lidar mounting with respect to the nacelle. In one of the two cases, larger deviations are seen in the turbulence level around the wake core. The reason of this discrepancy is not fully understood yet, but it is expected to be the consequence of the averaging procedure of the lidar, potentially attenuating in particular the small scale fluctuating part of the wind velocity, thus reducing the turbulence level around the wake core. However, the wake characteristics is very close to the computations, giving high confidence in both the measuring techniques and the CFD LES ACL model.

A subsequent analysis of merged wakes, as part of the DSF FlowCenter project, will comprise a set-up where both up and downstream turbines are mounted with synchronized lidar's and where the downstream lidar has a very high spatial and temporal resolution with a laser pattern optimized for wake measurement. Thus this analysis will not only benefit from the overall increased resolution, but the use of an additional upstream lidar system will give detailed knowledge of the single wake inflow to the downstream turbine. In the context of full wakes, it would be then possible to investigate the added wake turbulence and deficit generated by the downstream turbine. It will also be possible to investigate the turbulent content of a merged wake, its meandering, expansion and recovery in more detail.

6 Acknowledgments

Bibliography

[1] S. T. Frandsen. Turbulence and turbulence generated structural loading in wind turbine clusters. *Risø-R-1188(EN), Risø National Laboratory, Roskilde, Denmark*, 2007.

[2] N. O. Jensen. A note on wind turbine interaction. *Risø-M-2411, Risø National Laboratory, Roskilde, Denmark*, 1983.

[3] S. Ott, J. Berg, and M. Nielsen. Linearized CFD models for wakes. *Risø-R-1772(EN). Risø National Laboratory, Roskilde, Denmark*.

[4] G. C. Larsen, H. Aa. Madsen, K. Thomsen, and T. J. Larsen. Wake Meandering: A Pragmatic Approach. *Wind energy*, pages 11:377–395, 2008.

[5] F. Bingöl, G. C. Larsen, and J. Mann. Lidar Measurements of Wake Dynamics, Part 1: One-dimensional scanning. *Wind energy 13, 51-61*, 2010.

[6] G. España, S. Aubrun, S. Loyer, and P. Devinant. Wind tunnel study of the wake meandering downstream of a modeled wind turbine as an effect of large scale turbulent eddies. *Submitted for Journal of Wind Engineering and Industrial Aerodynamics*, 2011.

[7] H. Aa. Madsen, G. C. Larsen, T. J. Larsen, N. Troldborg, and Mikkelsen R. Calibration and Validation of the Dynamic Wake Meandering Model for Implementation in an Aeroelastic Code. *Journal of Solar Energy Engineering*, 2010.

[8] T. J. Larsen, H. Aa. Madsen, G. C. Larsen, and K. S. Hansen. Validation of the Dynamic Wake Meander Model for Loads and Power Production in the Egmond aan Zee Wind Farm. *Submitted to Wind energy, 2012*.

[9] G. C. Larsen, J. Mann, K. S. Hansen, K. Enevoldsen, and F. Bingöl. Full-scale measurements of wind turbine wake turbulence. Proceedings of Torque 2010. The Science of Making Torque From Wind Energy. *Heraklion, Greece*, pages 391–405, 2010.

[10] T. M. Fletcher and R. E. Brown. Simulation of wind turbine wake interaction using the transport vorticity model. *Wind Energy*, 2009.

[11] N. Troldborg, G. C. Larsen, H. Aa. Madsen, K. S. Hansen, J. N. Sørensen, and R. Mikkelsen. Numerical Simulations of Wake Interaction between Two Wind Turbines at Various Inflow Conditions. *Wind Energy, 14, doi: 10.1002/we.433*, pages 859–876, 2010.

[12] R. C. Storey, S. E. Norris, K. A. Stol, and J. E. Cater. Large Eddy Simulation of Dynamically Controlled Wind Turbines using Actuator Discs. *50th AIAA Aerospace, Science Meeting January 2012, Nashville, Tennessee*, 2012.

[13] S. Lee, M. Churchfield, P. Moriarty, J. Jonkman, and J. Michalakes. Atmospheric and Wake Turbulence Impacts on Wind Turbine Fatigue Loadings. *50th AIAA Aerospace, Science Meeting January 2012, Nashville, Tennessee*, 2012.

[14] S. Ivanell. Numerical Computation of Wind Turbine Wakes, PhD Thesis. *Royal Institute of Technology, Stockholm, Gotland University, Sweden*, 2009.

[15] M. J. Churchfield, S. Lee, P. Moriarty, L. A. Martinez, S. Leonardi, G. Vijayakumar, and JG. Brasseur. A Large-Eddy Simulation of Wind-Plant Aerodynamics. *50th AIAA Aerospace, Science Meeting January 2012, Nashville, Tennessee*, 2012.

[16] G. C. Larsen, H. Aa. Madsen, T. J. Larsen, P.-E. Réthoré, and Peter Fuglsang. TOPFARM - A platform for wind farm topology optimization. *Book of Abstracts / Editor: Ivanell S. - Wake conference, Visvy, Sweden*, pages 40–42, 2011.

[17] P. Lindelöw-Marsden. Upwind D1. Uncertainties in wind assessment with LIDAR. *Risø-R-1681 (EN), Risø National Laboratory, Roskilde, Denmark*, 2009.

[18] G. C. Larsen, K. S. Hansen, N. Troldborg, J. Mann, K. Enevoldsen, and F. Bingöl. An attempt to characterize the structure of wake turbulence using a combined experimental and numerical approach. *Conference on Turbulence IV, Bertinoro (IT), 19-22 Sep*, 2010.

[19] J. A. Michelsen. Block Structured Multigrid solution of 2D and 3D elliptic PDE's. Dept. of Fluid mechanics, DTU. *AFM 94-05*, 1994.

[20] N. N. Sørensen and W. Z. Shen. General purpose flow solver applied to flow over hills, PhD Thesis, Risø National Laboratory. *Wind energy*, 1995.

[21] J. N. Sørensen and W. Z. Shen. Numerical modeling of Wind Turbine Wakes, Fluids Engineering, Vol 124, Issue 2. *Wind energy*, 2002.

[22] J. Mann. The spatial structure of neutral atmospheric surface-layer turbulence. *Journal of fluid mechanics*, pages 273, 141–168, 1994.

[23] F. Zahle and N. N. Sørensen. Rotor Aerodynamics in Shear Flow. *Proceedings of the 2008 EWEC Conference, Bruxelles*, 2008.